ADVANCED ROBOTICS, 2016
http://dx.doi.org/10.1080/01691864.2016.1145596

FULL PAPER

New evaluation framework for human-assistive devices based on humanoid robotics

Ko Ayusawa[a], Eiichi Yoshida[a], Yumeko Imamura[a] and Takayuki Tanaka[b]

[a]CNRS-AIST JRL (Joint Robotics Laboratory), UMI3218/RL, Intelligent Systems Research Institute, National Institute of Advanced Industrial Science and Technology (IS-AIST), Tsukuba, Japan; [b]Graduate School of Information Science and Technology, Hokkaido University, Sapporo, Japan

ABSTRACT

This paper presents the new application of a humanoid robot as an evaluator of human-assistive devices. The reliable and objective evaluation framework for assistive devices is necessary for making industrial standards in order that those devices are used in various applications. In this framework, we utilize a recent humanoid robot with its high similarity to humans, human motion retargeting techniques to a humanoid robot, and identification techniques of robot's mechanical properties. We also show two approaches to estimate supporting torques from the sensor data, which can be used properly according to the situations. With the general formulation of the wire-driven multi-body system, the supporting torque of passive assistive devices is also formulated. We evaluate a passive assistive wear 'Smart Suit Lite (SSL)' as an example of device, and use HRP-4 as the humanoid platform.

ARTICLE HISTORY
Received 22 March 2015
Revised 4 August 2015 and 2 January 2016
Accepted 13 January 2016

KEYWORDS
Humanoid robot; assistive device evaluation; identification; joint torque estimation

1. Introduction

Recent development of human-assistive devices is attracting attention in several nations entering the super-aged society. In order to support the daily life of elderly people and to relieve the burden on nursing care workers, assistive devices have been intensively studied and developed.[1,2] Contrary to such demands, those technologies are experiencing slow development and implementation because of the difficulty of evaluation. The reliable and objective evaluation framework is necessary when making industrial standards for those products to be used by elderly people and nursing care workers. When evaluating assistive devices and making those standards, the assistive performance on human body needs to be quantified. However, the evaluation by human measurement still remains several bottlenecks: variation of human subjects, gathering appropriate subjects, reproducing the same motions, and ethical procedures for the experiments. Even after overcoming those problems, the most significant problem is the difficulty in measuring and quantifying the internal force information like joint torques or muscle tensions. It is true that recent development of human motion capture enables the quantitative evaluation of joint trajectories, but on the other hand, the forces generated inside human body are difficult to be directly measured. The common way has been to estimate it with motion capture and force plate measurement.[3] In principle, those estimation methodologies of multiple contact forces have always been facing the redundancy problem. Especially, when the subject wears the suit-type device, it is of great difficulty to extract the force effects of the device on the body. Humanoid robots with their internal sensors are, instead, expected to complement the conventional evaluation scheme of human subjects with the additional information about internal forces,[4] since they are uninfluenced by the above issues.

Our purpose is to develop the reliable evaluation framework of human-centered design products including assistive devices, and our final goal is industrial promotion by making industrial standards about not only safety issue but also effect on humans. To this end, this paper aims at developing a methodology of using humanoid robots instead of human subjects, in order to evaluate assistive devices by the quantitative measures from their internal sensors. There are also several expected advantages; humanoid robots can physically simulate usage of the device in real life in a similar manner to humans, they can repeat exactly the same motions with providing the repeatability of experiments and evaluation, ethical problems can be cleared for experiments. When evaluating the devices with a humanoid robot, the several issues have to be considered.

CONTACT Ko Ayusawa k.ayusawa@aist.go.jp
This paper is selected as the "Cutting Edge of Robotics in Japan" by the Editorial Committee of Advanced Robotics.

First of all, the morphology of the robot needs to be almost same as that of a human, in order that the robot can use the devices which are originally designed for human morphology. The correspondence of body parts between them also makes it easier to validate the effect on humans. Some recent humanoid robots like HRP-4C [5] and HRP-4 [6] whose structure and dimension are close to human can fulfill such requirements. In spite of the simplified kinematic structure of humanoid robots, studies in biomechanics have demonstrated that it is sufficient to estimate the load at lower back.[7]

Secondly, this application requires that the robot should mimic human motion as close as possible to original features. We here employ the technique of motion retargeting that have been widely studied to design character animations in the field of computer graphics, or to generate robot motions.[8–10]

Finally, the accurate measurement or estimation of joint torques is required because joint torque quantifies the supportive effect of reducing the load applied to joints. Since it is still difficult to integrate joint torque sensors into a lightweight humanoid such as HRP-4, we have to rely on input signals of electric motors. Identification technique [11] is therefore important to estimate the joint torque accurately.

Based on some pilot studies,[4,12] this paper presents the new application framework of a humanoid robot as an evaluator of assistive devices. In this framework, we utilize several technologies developed in humanoid robotics: a recent humanoid robot with high similarity to humans, human motion retargeting techniques to a humanoid robot, and identification techniques of the mechanical properties of a humanoid robot: inertial parameters (mass, center of mass, and inertia tensor) of each link, joint friction coefficients, motor constants, and sensor offsets of each joint. We also show the two approaches to estimate the supporting effects from the sensor data of a robot. As an example of assistive device, we evaluate a passive assistive wear 'Smart Suit Lite (SSL)' that supports the load at the lower back with the elastic bands.[2] SSL began to be widely used through test marketing to reduce load of workers in such application fields as agriculture, horse training and nursing care.[13,14] Although the questionnaires to users showed that they feel a smaller load at their back when using SSL,[2] we believe quantitative evaluation is necessary to validate its supportive effect and also to meet industrial standards in future. Quantitative evaluation framework that we propose in this paper can also contribute to product design improvement to offer better supportive effects.

2. Flow of evaluation of assistive device with humanoid robot

Though the most common way to evaluate human-assistive devices is, of course, the measurement of human subjects, it contains several difficulties as follows:

- recruitment of human subjects in specified range of gender, age, degree of disability.
- reproduction of the same motions for specific evaluation.
- ethical procedures for the experiments.
- measurement of forces generated inside body.

Since humanoid robots are not influenced by the above issues, this paper aims at developing a methodology of using them instead of human subjects. The expected advantages of this replacement are summarized as followings:

- Humanoid robots with the same morphology as humans can physically simulate usage of the device in a similar manner to humans.
- Since robots can repeat exactly the same motions, they can realize the repeatability of experiments and evaluation.
- Ethical problems can be cleared for experiments with risks of injury.
- They can provide quantitative measures such as joint trajectories, torques or applied forces.

This framework requires that the humanoid robot has to be almost the same morphology as a human. The examples of such robots are as shown in Figure 1. HRP-4C [5] is one of the robots which fulfill the requirement. The robot is 1.58 m in height and 43 kg in weight, featuring its geometric parameters close to the measured average of women of 19–29 years old in Japan, and can wear clothes or devices designed for humans. HRP-4 was also developed as a commercial robot based on the design of HRP-4C. In this paper, we use HRP-4 as an evaluator of assistive devices by removing its hard plastic cover and clothing a soft suit, to realize soft surface like a human. Strictly speaking, the joint configuration of such a robot is still different from that of the human body. However, the human model used in the inverse dynamics analysis is also often simplified [15] because of some practical issues. Those simplified models are actually used in biomechanics, for instance to estimate the load in lower back.[7]

Here, is the evaluation flow using those humanoid robots (Figure 2):

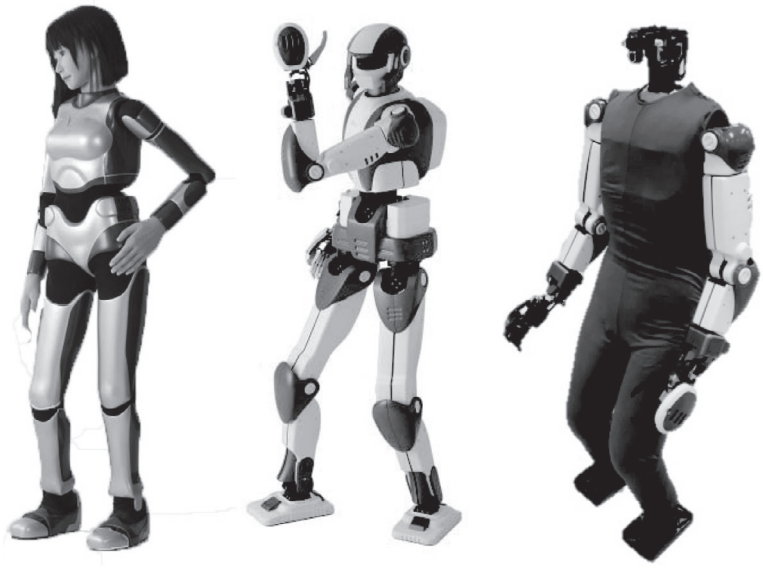

Figure 1. Humanoid robot HRP-4C (Left), HRP-4 (Middle), and HRP-4 with a soft suit instead of hard plastic cover (Right).

(S1) Measurement of human motion data.
(S2)
  (a) Retargeting human motion to the humanoid robot.
  (b) Identification of the mechanical parameters of the robot by experimental data.
(S3) Estimation of supporting torques of the devices.
(S4) Evaluation of the devices by using the estimated results.

Even though we evaluate the devices with a humanoid robot, we have to define the human motion which should be performed in the evaluation. In order to prepare them in step 1(S1), we utilize the human motion capturing.

Motion capture data is widely used for creating the motion of human-like characters in the field of computer graphics.[8] Some robotics studies demonstrated their created motion on a real human-like and human-sized robot. Japanese traditional dancing has been realized on humanoid HRP-2, based on the motion capture data of a professional dancer.[9] Our application requires that the robot should mimic human motion without modifying the kinematic and dynamic characteristics of the original motion. In step 2(a), we use a retargeting technique,[10] which is adapted to reproduction of whole-body motion preserving many kinematic and dynamic constraints for the humanoid.

The accurate measurement or estimation of joint torques is important, which usually requires the joint torque sensors or the identification of the mechanical parameters of each joint. Even though the recent development of the torque sensors enable them on a humanoid robot [16] and they are expected as a useful technology for our application, it will still take time to decrease the weight and size of them to keep human morphology as a human evaluator. In this paper, the joint torques are estimated from the inertial parameters, motor constants, gear-ratio, etc. provided by manufacturers. However, they are not necessarily accurate because of the uncertain elements like frictions, and can change when, for example, robot carries the objects, the temperature condition of actuators changes, etc. We thus identify those parameters of the robot in step 2(b). The detailed procedure is shown in Section 3.

The equations of motion of the robot with and without the device are simplified as follows:

$$\boldsymbol{\tau}_{\mathrm{dyn}}\left(\boldsymbol{x}^{\text{with device}}, \boldsymbol{\phi}\right) = \boldsymbol{\tau}_{\mathrm{actuator}}\left(\boldsymbol{y}^{\text{with device}}, \boldsymbol{\xi}\right) + \boldsymbol{\tau}_{\mathrm{support}} \quad (1)$$

$$\boldsymbol{\tau}_{\mathrm{dyn}}\left(\boldsymbol{x}^{\text{without device}}, \boldsymbol{\phi}\right) = \boldsymbol{\tau}_{\mathrm{actuator}}\left(\boldsymbol{y}^{\text{without device}}, \boldsymbol{\xi}\right) \quad (2)$$

where $*^{\text{with device}}$ and $*^{\text{without device}}$ mean the variables when with and without the device respectively, $\boldsymbol{x}$ indicates the robot's generalized coordinates and their derivatives, $\boldsymbol{y}$ shows the actuators' inputs, $\boldsymbol{\phi}$ represents the inertial parameters of the robot, $\boldsymbol{\xi}$ denotes the parameters of the actuator models including frictions, $\boldsymbol{\tau}_{\mathrm{dyn}}$ means the torques coming from the pure inertial effect, $\boldsymbol{\tau}_{\mathrm{actuator}}$ is the torque generated from the actuators including the frictions, and $\boldsymbol{\tau}_{\mathrm{support}}$ indicates the supporting (external) torque of the device.

There are two approaches to estimate the supporting torques in step 3 as follows:

(A) Perform the same motion with and without the device, respectively (i.e. $\boldsymbol{x}^{\text{with device}} \approx \boldsymbol{x}^{\text{without device}}$). Then, $\boldsymbol{\tau}_{\mathrm{dyn}}\left(\boldsymbol{x}^{\text{with device}}, \boldsymbol{\phi}\right) \approx \boldsymbol{\tau}_{\mathrm{dyn}}\left(\boldsymbol{x}^{\text{without device}}, \boldsymbol{\phi}\right)$

holds. By utilizing Equations (1) and (2), we can compute the supporting torques as follows:

$$\boldsymbol{\tau}_{\text{support}} \approx \boldsymbol{\tau}_{\text{actuator}}\left(\boldsymbol{y}^{\text{without device}}, \widehat{\boldsymbol{\xi}}\right) - \boldsymbol{\tau}_{\text{actuator}}\left(\boldsymbol{y}^{\text{with device}}, \widehat{\boldsymbol{\xi}}\right) \quad (3)$$

where $\widehat{\boldsymbol{\xi}}$ means the identified parameters of the actuators and the frictions.

(B) Compute the difference in Equation (1) between the measured joint torques and those estimated from the simulation model whose mechanical parameters were identified in advance:

$$\boldsymbol{\tau}_{\text{support}} \approx \boldsymbol{\tau}_{\text{dyn}}\left(\boldsymbol{x}^{\text{with device}}, \widehat{\boldsymbol{\phi}}\right) - \boldsymbol{\tau}_{\text{actuator}}\left(\boldsymbol{y}^{\text{with device}}, \widehat{\boldsymbol{\xi}}\right) \quad (4)$$

where $\widehat{\boldsymbol{\phi}}$ is the identified inertial parameters of the robot without the device.

Figure 3 illustrates the two approaches. In approach (A), we need $\boldsymbol{y}^{\text{with device}}$, $\boldsymbol{y}^{\text{without device}}$ and $\widehat{\boldsymbol{\xi}}$. Approach (B) requires $\boldsymbol{x}^{\text{with device}}$, $\boldsymbol{y}^{\text{with device}}$, $\widehat{\boldsymbol{\xi}}$ and $\widehat{\boldsymbol{\phi}}$. Model parameters $\widehat{\boldsymbol{\xi}}$ and $\widehat{\boldsymbol{\phi}}$ are obtained from the identification: step 2(b). Other variables need to be measured by the internal sensors. The strong merit of approach (A) is cancelling the unmodeled friction forces in $\boldsymbol{\tau}_{\text{actuator}}$; there is some possibility to eliminate them by the subtraction of Equation (3). However, the demerit is that the same motion has to be performed between with and without the device. Some devices are originally designed so that the human should perform the different motion with and without them. In this case, approach (A) is difficult to be used. Approach (B) is the general formulation; the accurate model of the robot (i.e. the identification of mechanical parameters) has to be required. Unlike approach (A), the supporting torque can be extracted directly from the recorded data with the device by approach (B).

Finally, in step 4, the assistive device is evaluated by the obtained supporting torques. In this paper, we evaluate a passive assistive wear 'SSL',[2] and identify the stiffness of SSL band from the experimental data of the robot. The detail of the modeling of SSL and the identification procedure is shown in Section 4.

The merits and the demerits of the evaluation with human experiments and that with a humanoid robot are summarized in Table 1. One note is that the proposed framework also has some limitations. For example, the evaluation of the physiological or psychological effects of the device on a human, of course, needs human experiments. The proposed framework is focusing on the quantitative evaluation of mechanical effects on a human, and should be used for such a purpose.

3. Identification of humanoid robot

This section shows the procedure to identify the mechanical parameters of a humanoid robot from its internal sensors. Though the methodology is based on the identification of classical manipulators,[11,17] it is combined with the identification using base-link dynamics.[18] Based on our pilot study,[12] the method can compensate the static frictions additionally, which leads to increase performance of the estimation of joint torques.

3.1. Basic formulation

The equations of motion of a humanoid robot are formulated as [19]:

$$\begin{bmatrix} \boldsymbol{M}_{oo} & \boldsymbol{M}_{oj} \\ \boldsymbol{M}_{oj}^T & \boldsymbol{M}_{jj} \end{bmatrix} \begin{bmatrix} \ddot{\boldsymbol{q}}_o \\ \ddot{\boldsymbol{\theta}} \end{bmatrix} + \begin{bmatrix} \boldsymbol{c}_o \\ \boldsymbol{c}_j + \boldsymbol{\tau}_f \end{bmatrix} = \begin{bmatrix} \boldsymbol{0} \\ \boldsymbol{\tau} \end{bmatrix} + \sum_{k=1}^{N_c} \begin{bmatrix} \boldsymbol{K}_{ok}^T \\ \boldsymbol{K}_{ck}^T \end{bmatrix} \boldsymbol{F}_k^{\text{ext}} \quad (5)$$

where

- $\boldsymbol{q}_o \in SE(3)$ is the vector of the generalized coordinates which represent the position and orientation of the base-link,
- $\boldsymbol{\theta} \in \mathbb{R}^{N_J}$ is the vector of joint angles,
- N_J is the number of degree of freedom (DOF),
- N_c is the number of contact points with the environment,
- $\boldsymbol{M}_{oo} \in \mathbb{R}^{6\times 6}$, $\boldsymbol{M}_{oj} \in \mathbb{R}^{6\times N_J}$, and $\boldsymbol{M}_{jj} \in \mathbb{R}^{N_J\times N_J}$ represent the inertia matrices,
- $\boldsymbol{c}_o \in \mathbb{R}^6$ mean the bias force vector including centrifugal, Coriolis, and gravity forces acting on the base-link, and $\boldsymbol{c}_j \in \mathbb{R}^{N_J}$ is that for the joints,
- $\boldsymbol{\tau} \in \mathbb{R}^{N_J}$ is the vector of joint torque,
- $\boldsymbol{\tau}_f \in \mathbb{R}^{N_J}$ is the vector of joint friction torques,
- $\boldsymbol{F}_k^{\text{ext}} \in \mathbb{R}^6$ represents the vector of external forces exerted to the system at contact k,
- $\boldsymbol{K}_k \triangleq [\boldsymbol{K}_{ok}\ \boldsymbol{K}_{ck}] \in \mathbb{R}^{6\times(6+N_J)}$ is the Jacobian matrix associated to contact k and of the orientation of the contact link with respect to generalized coordinates.

The upper part of Equation (5) corresponds with the equations of motion of the base-link, and the lower one means those of joints. Since a humanoid robot is not fixed to the environment, the generalized input forces which actuate the six DOF of its base-link are always equal to zero; the upper part of Equation (5) does not contain the joint torque and friction.

$\boldsymbol{\tau}$ is defined as the following linear identification model of motors:

$$u_{(i)} k_{T(i)} + \tau_{o(i)} = \tau_i \quad (6)$$

Table 1. Comparison between the evaluation with human measurement and that with humanoid measurement.

	Human	Humanoid
Non-requirement of ethical procedure	No	Yes
Non-variation among subjects	No	Yes
Motion repeatability	No	Yes
Possibility of internal force measurement	Difficult	Yes
Possibility of physiological evaluation	Yes	No
Possibility of psychological evaluation	Yes	No
Similarity to human body	–	Needed
Retargeting and control	–	Needed
Accurate modeling	–	Needed

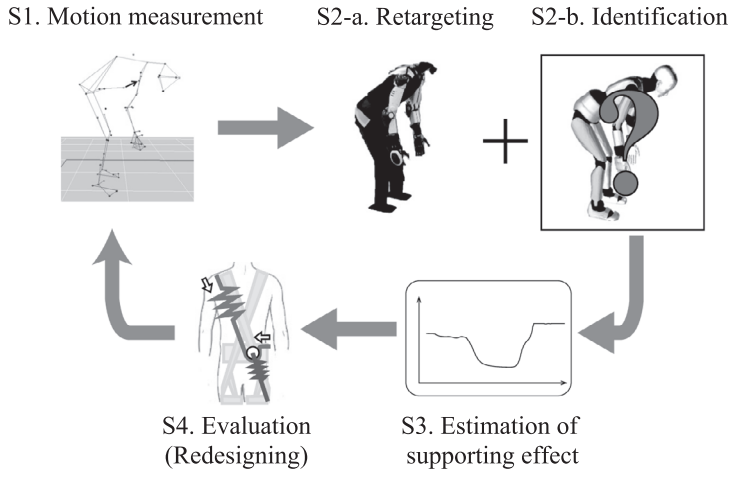

Figure 2. Outline of framework to evaluate assistive devices by using a humanoid robot.

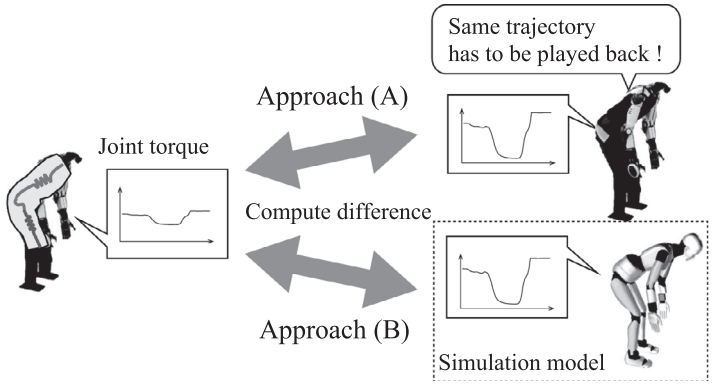

Figure 3. Two approaches to estimate supporting effect. Approach (A) estimates the effect from Equation (3). Approach (B) computes by utilizing Equation (4).

where $*_{(i)}$ means ith element of vector $*$, $\boldsymbol{u} \in \mathbb{R}^{N_J}$ is the vector of electrical currents, $\boldsymbol{k}_T \in \mathbb{R}^{N_J}$ is the vector of motor constants which contains the squared gear ratio, and $\boldsymbol{\tau}_o \in \mathbb{R}^{N_j}$ is the vector of offset torques due to motor current amplifier offset.

Let $\boldsymbol{\tau}_f$ contain the following frictions:

$$\tau_{f(i)} = \dot{\theta}_{(i)} k_{d(i)} + \mathrm{sgn}(\dot{\theta}_{(i)}) \tau_{c(i)} + \left(1 - |\mathrm{sgn}(\dot{\theta}_{(i)})|\right) \tau_{s,(i)} \tag{7}$$

where $\boldsymbol{k}_d \in \mathbb{R}^{N_J}$ is the vector of viscous friction coefficients, $\boldsymbol{\tau}_c \in \mathbb{R}^{N_J}$ is the vector of Coulomb frictions, and $\boldsymbol{\tau}_s \in \mathbb{R}^{N_J}$ is the vector of static frictions, Though $\boldsymbol{\tau}_c$, strictly speaking, depends on the constraint forces acting on the joint axis, let us assume that the actuator-side friction is dominant and $\boldsymbol{\tau}_c$ is constant.

$\tau_{s(i)}$ is also not constant, and their absolute values are also upper bounded by the maximum static frictions $\tau_{s(i)}^{\max}$. We also assume that the actuator-side friction is

dominant and rigid servo control leads the bias, and let $|\tau_{s(i)}| \approx \tau_{s(i)}^{\max}$ holds during the identification procedure. Let us assume that the sign of $\boldsymbol{\tau}_s$ depends on the sum of the residual forces as follows:

$$\tau_{s(i)} \approx \mathrm{sign}(\widehat{\tau}_{s,j})\tau_{s(i)}^{\max} \tag{8}$$

$$\widehat{\boldsymbol{\tau}}_s \triangleq \widehat{\boldsymbol{\tau}} - \widehat{\boldsymbol{c}}_j + \sum_{k=1}^{N_c} \boldsymbol{K}_{ck}^T \boldsymbol{F}_k^{\mathrm{ext}} \tag{9}$$

where sign(.) denotes the sign function. Before the identification, we cannot know $\boldsymbol{\tau}$ and $\boldsymbol{c}_j$ because they contains unknown parameters. Therefore, we estimate them by using the a priori knowledge which can be obtained, for example, from CAD data of the model; $\widehat{\boldsymbol{\tau}}$ and $\widehat{\boldsymbol{c}}_j$ are the estimated values.

In the following discussion, let us define the second term of the right-hand side of Equation (5) as follows:

$$\begin{bmatrix} \boldsymbol{F}_o \\ \boldsymbol{F}_j \end{bmatrix} \triangleq \sum_{k=1}^{N_c} \begin{bmatrix} \boldsymbol{K}_{ok}^T \\ \boldsymbol{K}_{ck}^T \end{bmatrix} \boldsymbol{F}_k^{\mathrm{ext}} \tag{10}$$

where $\boldsymbol{F}_o$ and $\boldsymbol{F}_j$ mean the total external forces acting on the base-link and the joints, respectively.

The equations of motion of multi-body systems can be written in a linear form with respect to the inertial parameters,[11,17] and Equation (11) can be transformed from Equation (5).

$$\begin{bmatrix} \boldsymbol{Y}_o & \boldsymbol{O} \\ \boldsymbol{Y}_j & \boldsymbol{Z} \end{bmatrix} \begin{bmatrix} \boldsymbol{\phi} \\ \boldsymbol{\xi} \end{bmatrix} = \begin{bmatrix} \boldsymbol{F}_o \\ \boldsymbol{F}_j \end{bmatrix} \tag{11}$$

where

- $\boldsymbol{\phi} \in \mathbb{R}^{N_\phi}$ is the vector of the minimum set of inertial parameters (or base parameters) which represents the equations of motions,[20]
- $\boldsymbol{\xi} \triangleq [\boldsymbol{k}_T^T \ \boldsymbol{k}_d^T \ \boldsymbol{\tau}_c^T \boldsymbol{\tau}_s^{\max T} \boldsymbol{\tau}_o^T]^T$ contains the parameters about viscous, Coulomb, static frictions, the motor constant, and the offset torque of the joints, and let $\boldsymbol{\xi}$ be called 'joint parameters' in the following discussion,
- $\boldsymbol{Y}_o$ and $\boldsymbol{Y}_j$ are the coefficient matrices (or regressor matrices) of $\boldsymbol{\phi}$,
- $\boldsymbol{O}$ means a zero matrix,
- $\boldsymbol{Z}$ is the regressor matrix of $\boldsymbol{\xi}$ as follows:

$$\begin{aligned} \boldsymbol{Z} \triangleq [&\mathrm{diag}(\boldsymbol{u})\mathrm{diag}(\dot{\boldsymbol{q}}_j)\mathrm{sgn}(\mathrm{diag}(\dot{\boldsymbol{q}}_j)) \\ &(\boldsymbol{I} - \mathrm{sgn}(\mathrm{diag}(\dot{\boldsymbol{q}}_j)))\mathrm{sgn}(\mathrm{diag}(\widehat{\boldsymbol{\tau}}_c))\boldsymbol{I}] \end{aligned} \tag{12}$$

where $\boldsymbol{I}$ is an identify matrix, $\mathrm{diag}(\boldsymbol{x})$ means the matrix whose diagonal elements is equal to those of $\boldsymbol{x}$.

Equation (11) is the basic formulation used for identification. When assuming that the geometric parameters like link lengths are known and $\boldsymbol{\phi}$ and $\boldsymbol{\xi}$ are constant unknown values, Equation (11) is linear with respect to the unknown parameters.

It is known that $\boldsymbol{\phi}$ of a legged system is identifiable only from the equations of the base-link.[18] After $\boldsymbol{\phi}$ is identified from the upper part of Equation (11), the parameter set of each joint among $\boldsymbol{\xi}$ can be individually identified from the equation of the corresponding joint. Thus, $\boldsymbol{\phi}$ and $\boldsymbol{\xi}$ are structurally identifiable from Equation (11).

3.2. Basic flow of identification

Let us identify the parameters using the following sensors:

- joint encoders which measure $\boldsymbol{\theta}$,
- a gyro and an accelerometer which obtain $\ddot{\boldsymbol{p}}_o$ and $\boldsymbol{\omega}_o$,
- force/moment sensors which detects $\boldsymbol{F}_k^{\mathrm{ext}}$,
- motor current sensors measuring $\boldsymbol{u}$

where $\ddot{\boldsymbol{p}}_o$ is the linear acceleration containing gravity acceleration with respect to the sensor coordinate, $\boldsymbol{\omega}_o$ is the angular velocity with respect to the sensor coordinate.

Let us select the link, which has the gyro and the accelerometer, as the base-link in Equation (11). When representing the upper part of Equation (11) with respect to its local coordinate system, Equation (11) does not include $\boldsymbol{q}_0$, $\dot{\boldsymbol{p}}_0$. Since $\ddot{\boldsymbol{p}}_o$ contains the gravity acceleration with respect to the local coordinate, $\boldsymbol{Y}_o$, $\boldsymbol{Y}_j$, $\boldsymbol{Z}$, $\boldsymbol{F}_o$ and $\boldsymbol{F}_j$ can be computed by $\boldsymbol{\theta}$, $\ddot{\boldsymbol{p}}_o$, $\boldsymbol{\omega}_o$, and their numerical derivatives. In order to identify the parameters, by sampling Equation (11) from the sensor data, and we have:

$$\begin{bmatrix} \widehat{\boldsymbol{Y}}_o^{(t)} & \boldsymbol{O} \\ \widehat{\boldsymbol{Y}}_j^{(t)} & \widehat{\boldsymbol{Z}}^{(t)} \end{bmatrix} \begin{bmatrix} \boldsymbol{\phi} \\ \boldsymbol{\xi} \end{bmatrix} = \begin{bmatrix} \widehat{\boldsymbol{F}}_o^{(t)} \\ \widehat{\boldsymbol{F}}_j^{(t)} \end{bmatrix} + \begin{bmatrix} \boldsymbol{e}_o^{(t)} \\ \boldsymbol{e}_j^{(t)} \end{bmatrix} \tag{13}$$

where notation $\widehat{\boldsymbol{x}}^{(t)}$ means the value which computed from tth sample of sensor data, and $\boldsymbol{e}_o$ and $\boldsymbol{e}_j$ are the errors.

The basic approach of the identification is the least squares method:

$$\min_{\boldsymbol{\phi},\boldsymbol{\xi}} \ h = \sum_{t}^{N_T} \left(\boldsymbol{e}_o^{(t)T} \boldsymbol{W}_o \boldsymbol{e}_o^{(t)} + \boldsymbol{e}_j^{(t)T} \boldsymbol{W}_j \boldsymbol{e}_j^{(t)} \right) \tag{14}$$

where N_T is the number of the samples, $\boldsymbol{W}_o \in \mathbb{R}^{6\times 6}$ and $\boldsymbol{W}_j \in \mathbb{R}^{N_J \times N_J}$ are weighting factors and diagonal matrices. They can be designed according to the variance of the measured force or moment in each equation. As the problem is the quadratic form, the analytical solution of the problem can be computed.

3.3. Implementation

When identifying the parameters, we often face the following problems:

- design of 'persistent excitation (PE) trajectory' which can identify the whole parameters,[21]
- inequality constraints about the physical consistency of the parameters.[22]

Let us assume that PE trajectories cannot always be obtained, and let us know the a priori knowledge which can be obtained, for example, from CAD data of the model. In the similar manner as the method,[23] we try to obtain all the standard parameters by utilizing a priori knowledge. In order to avoid overfitting problem under poor excitation, we solve the following least squares with the a priori knowledge:

$$\min_{\boldsymbol{\phi},\boldsymbol{\xi}} \; h + (\boldsymbol{\phi} - \boldsymbol{\phi}^{ref})^T \boldsymbol{W}_\phi (\boldsymbol{\phi} - \boldsymbol{\phi}^{ref}) + (\boldsymbol{\xi} - \boldsymbol{\xi}^{ref})^T \boldsymbol{W}_\xi (\boldsymbol{\xi} - \boldsymbol{\xi}^{ref}) \tag{15}$$

where $\boldsymbol{W}_\phi \in \mathbb{R}^{N_B \times N_B}$ and $\boldsymbol{W}_\xi \in \mathbb{R}^{3N_J \times 3N_J}$ are weighting factors and diagonal matrices. $\boldsymbol{\phi}^{ref}$ and $\boldsymbol{\xi}^{ref}$ are the a priori knowledge. When it is difficult to obtain the a priori knowledge like frictions, the values are set to zero.

Since the physical units of $\boldsymbol{\phi}$ and $\boldsymbol{\xi}$ are different, the weighting factors has to be normalized among them. Here, is the example to design the weighting factors:

$$\boldsymbol{W}_\phi = w_\phi \sigma_{\max}(\Lambda_\phi) \boldsymbol{I} \tag{16}$$

$$\boldsymbol{W}_\xi = \mathrm{diag}\left(\begin{bmatrix} w_T \sigma_{\max}(\boldsymbol{\Lambda}_T) \mathbf{1}_{N_j} \\ w_d \sigma_{\max}(\boldsymbol{\Lambda}_d) \mathbf{1}_{N_j} \\ w_c N_T \sigma_{\max}(\boldsymbol{W}_j) \mathbf{1}_{N_j} \\ w_s N_T \sigma_{\max}(\boldsymbol{W}_j) \mathbf{1}_{N_j} \\ w_o N_T \sigma_{\max}(\boldsymbol{W}_j) \mathbf{1}_{N_j} \end{bmatrix} \right) \tag{17}$$

$$\boldsymbol{\Lambda}_\phi \triangleq \sum_t^{N_T} \sum_t \left(\begin{bmatrix} \widehat{\boldsymbol{Y}}_o^{(t)T} & \widehat{\boldsymbol{Y}}_j^{(t)T} \end{bmatrix} \boldsymbol{W}_o \begin{bmatrix} \widehat{\boldsymbol{Y}}_o^{(t)} \\ \widehat{\boldsymbol{Y}}_j^{(t)} \end{bmatrix} \right) \tag{18}$$

$$\boldsymbol{\Lambda}_\xi \triangleq \sum_t^{N_T} \left(\mathrm{diag}(\boldsymbol{u}^{(t)}) \boldsymbol{W}_j \mathrm{diag}(\boldsymbol{u}^{(t)}) \right) \tag{19}$$

$$\boldsymbol{\Lambda}_d \triangleq \sum_t^{N_T} \left(\mathrm{diag}(\dot{\boldsymbol{\theta}}^{(t)}) \boldsymbol{W}_j \mathrm{diag}(\dot{\boldsymbol{\theta}}^{(t)}) \right) \tag{20}$$

where $\mathbf{1}_n \in \mathbb{R}^{n \times 1}$ is the vector whose elements are all one, $\sigma_{\max}(\boldsymbol{\Lambda})$ returns the maximum singular value of $\boldsymbol{\Lambda}$, and the normalized weighting scalar factors are w_ϕ, w_T, w_d, w_c, w_s, and w_o.

The solutions of Equation (15) are used as $\widehat{\boldsymbol{\phi}}$ and $\widehat{\boldsymbol{\xi}}$ in Equations (3) and (4). Those parameters are identified in advance by using the data when the robot does not wear an assistive device.

4. Modeling of passive power-assist devices

This section introduces the modeling of passive power-assist devices for simulation, and shows the example of the model of SSL. Though we can also make use of simulations to test different parameters settings and product configurations, they have to be compared and validated by using experiments to reflect the real situations. In this section, we also show the methodology of the identification of the simulation model from the experimental data.

4.1. General formulation of wire-based assistive devices

Nominal modeling of supporting mechanism of assistive devices has a great role to design, modify, and evaluate them. If a passive power-assist device consists of several elastic bands or belts, the supporting torques generated in human joints can be modeled by the same manner as the formulation of wire-driven multi-body systems. It is also related to the musculoskeletal analysis; the joint torques are generated by several muscles modeled as elastic wires.[3] We, therefore, can utilize the same formulation and framework which map the elastic forces to the joint torques, and prepare elastic model of each assistive device.

Each wire has several via points fixed on the rigid-body system. The supporting torques are formulated as follows:

$$\boldsymbol{\tau}_{\text{support}} = \sum_{i=1}^{N_l} \boldsymbol{J}_i^T f_i \tag{21}$$

where

- $\boldsymbol{\tau}_{\text{support}} \in \mathbb{R}^{N_J}$ is the vector of supporting torques,
- $f_i \in \mathbb{R}$ is the elastic force of ith wire,
- N_l is the number of wires,
- $\boldsymbol{J}_i \in \mathbb{R}^{1 \times N_J}$ is the Jacobian matrix of the length of ith wire:

$$\boldsymbol{J}_i \triangleq \frac{\partial l_i}{\partial \boldsymbol{\theta}} \tag{22}$$

- $l_i \in \mathbb{R}$ is the length of ith wire.

Since each wire consists of several line segments which are connected between the corresponding two via-points, length l_i can be computed as follows:

$$l_i = \sum_{j=2}^{N_{v,i}} || \boldsymbol{p}_{i,j} - \boldsymbol{p}_{i,j-1} || \tag{23}$$

where

- $N_{v,i} (> 1)$ is the number of via points of ith wire,

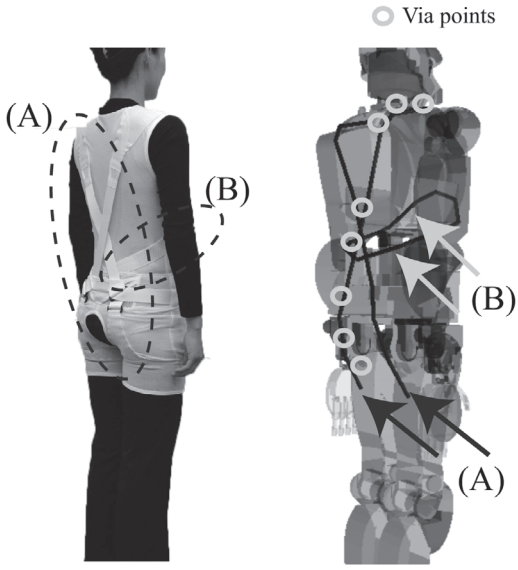

Figure 4. Overview of assistive wear 'Smart Suite Lite' (Left) and its computational wire model (Right). There are two wires which, respectively, have eight via points attached on the robot.

- $\boldsymbol{p}_{i,j} \in \mathbb{R}^3$ is the position of jth via point of ith wire, which is computed from the following forward kinematics computation:

$$\boldsymbol{p}_{i,j} = \boldsymbol{p}_{p(i,j)} + \boldsymbol{R}^{p(i,j)}_{p(i,j)} \boldsymbol{p}_{i,j} \tag{24}$$

- function $p(i,j)$ returns the index of the link where jth via point of ith wire is located,
- $\boldsymbol{p}_k \in \boldsymbol{R}^3$ and $\boldsymbol{R}_k \in SO(3)$ are the position and the orientation of link k, respectively,
- ${}^{p(i,j)}\boldsymbol{p}_{i,j} \in \boldsymbol{R}^3$ is the relative position of jth via point of ith wire with respect to the attached link coordinate.

4.2. Modeling and identification of the elastic model of SSL

The basic function of 'Smart Suit Lite (SSL)' [2] is to reduce the torque at the lower back by stretched two elastic bands fixed at the shoulders and thighs, which are shown as wire-(A) in the left figure of Figure 4. SSL also has the short bands which are fixed at the back and the chest: wire-(B) illustrated in Figure 4. Based on the pilot studies [4,12], they are also considered to evaluate the effect during the motion around the yaw-axis of waist. In order to represent the SSL bands, several via points per one band are located on the surface of the model of HRP-4. The location of via-points of wire-(A) is shown in the right side of Figure 4. Each via point is fixed on the corresponding link, and its position can be computed by the forward kinematics computation as mentioned before. Therefore, we modeled four elastic wires: two wires of type-(A) and two wires of type-(B).

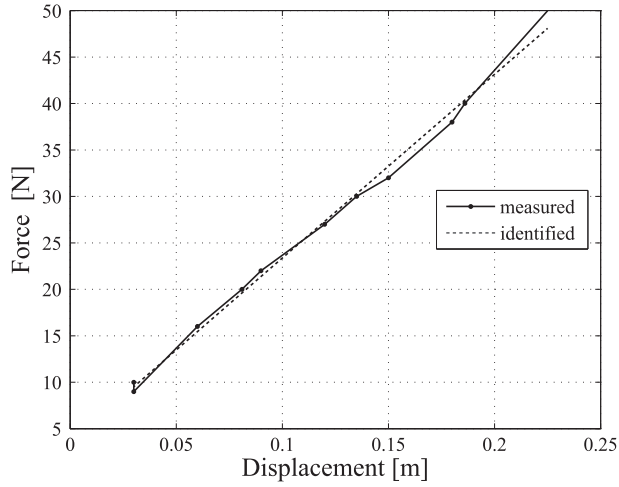

Figure 5. Experimental data of the relationship between the displacement and the elastic force of SSL band. The thin line shows the measured data, and dotted line shows the result by linear fitting.

The elastic force of each SSL band is formulated as a linear spring as follows:

$$f_i = \begin{cases} -k_i(l_i - l_{0,i}) & (l \geq l_{0,i}) \\ 0 & (l < 0) \end{cases} \tag{25}$$

where l_{i0} is the natural length and k_i is the stiffness of SSL band i.

Figure 5 shows the experimental data of the relationship between the length and the force of the SSL band corresponding to wire-(A) in Figure 4. The stiffness of the SSL band is $k_i = 197.8$ N/m, which is identified by solving linear regression problem. Though the experimental data of wire-(B) when wearing SSL is not available, in this paper, we assume that the stiffness of wire (B) is same as that of wire (A).

The supporting torques of SSL are computed from Equations (21) and (25). If the geometric parameters of the robot and the location of via points are known, $\boldsymbol{\tau}_{\text{support}}$ depends on the following constant parameters:

- stiffness k_i
- natural length $l_{0,i}$

Let us identify k_i and $l_{0,i}$ from the estimated supporting torques. The identification problem of them is written as:

$$\min_{\forall i\ k_i, l_{0,i}} \sum_t \left(|| \widehat{\boldsymbol{\tau}}_s^{(t)} - \widehat{\boldsymbol{J}}_i^{(t)} \widehat{f}_i^{(t)} || \right) \tag{26}$$

where $\widehat{\boldsymbol{\tau}}_s^{(t)}$ is the vector of the supporting torque at sample t, which is estimated from Equations (3) or (4). $\widehat{\boldsymbol{J}}_i^{(t)}$ is

computed by $\boldsymbol{\theta}^{(t)}$ and independent from k_i and $l_{0,i}$. $\widehat{f}_i^{(t)}$ is made of not only $\boldsymbol{\theta}^{(t)}$ but also k_i and $l_{0,i}$.

As can been seen from Equation (25), f_i is not linear with respect to $l_{i,0}$ because of the case statements. Equation (26) is not the quadratic problem unlike Equations (14) and (15). Since Equation (26) has no equality or inequality constraints, the problem can be solved by, for example, the quasi-Newton method.

5. Experiments

This section validates the proposed scheme. According to the flow shown in Section 2, we captured the human motions, and retargeted the motion to the humanoid robot. We also identified the parameters of the robot by checking the performance of the identification. The supporting effects were estimated from the two approaches as shown in Section 2, and were compared with the results of the simulation model. As mentioned in Section 1, the ground-truth values of the supporting effect are difficult to be obtained from human measurement. In this paper, we propose evaluating the accuracy of our framework in the indirect way as follows. The results of the supporting effects were used to identify the mechanical parameters of the device. Since we have the part of ground-truth mechanical parameters, the identified parameters were compared with them in order to validate the accuracy of the proposed scheme.

5.1. Human motion measurement and retargeting

The pilot experiments were conducted with humanoid robot HRP-4 [6] with a soft suit instead of hard plastic cover as shown in the right of Figure 1. The replacement of the hard cover with the soft suit is aimed to mimic human body surface. The geometric structure of HRP-4 is also designed to be close to the measured average of humans. Those characteristics lead that the robot can wear clothes or devices designed for humans. Figure 6 shows the overview when HRP-4 is wearing SSL.

The evaluation flow described in Section 2 was validated. In step 1(S1), the following two motions were recorded using motion capture systems:

(1) Bending forward from the waist holding a dumbbell (0.5 kg each) in the both hands (Figure 7). Let us call it 'bending motion'.
(2) Lifting up the object that is placed in front of the subject, and put it on the side by twisting the waist, and then put it back to the original position (Figure 8). Let it be called 'twisting motion'.

The bending motion was acquired by Vicon Motion Systems, and the twisting motion was recorded by Motion Analysis System. The reason of using the different systems is simply because the latter motion was additionally captured on a different date and in a different facility due to some technical problems. Both sampling rates were 200 frames per second. By utilizing the motion retargeting method,[10] in step 2-(A), the bending motion was converted to a trajectory feasible to HRP-4. The body structure between the captured subject and the robot were quite different when capturing the twisting motion. In the retargeting process, we utilize the technique of the identification of geometric parameters [24,25] in order to compensation of the difference.

Figure 6. Overview of HRP-4 wearing SSL.

5.2. Identification of HRP-4

We identified the inertial parameters and joint parameters of HRP-4 by solving Equation (15) in step 2-(B) of Section 2. Some retargeted trajectories were performed by HRP-4 without SSL. The a priori parameters used in Equation (14) were the inertial parameters provided by the manufacturer.

Let us check the performance of the identified parameters. Figure 9 shows three types of the external pitch-axis moment acting on the base-link during the bending motion. The first one is the moment obtained from the force sensors: the upper right-hand side of Equation (5). The others are those reconstructed from the dynamics model using the identified parameters and the CAD parameters, respectively: the upper left-hand side of Equation (5). The reconstructed moment from the identified model shows a better correlation with the measured one. We also computed the root mean square error (RMSE) of the reconstruction, which corresponds with $\boldsymbol{e}_o^{(t)}$ in Equation (13). When using the a priori parameters, RMSE is 3.57 Nm. On the other hand, when using the identified parameters, RMSE is smaller: 1.13 Nm.

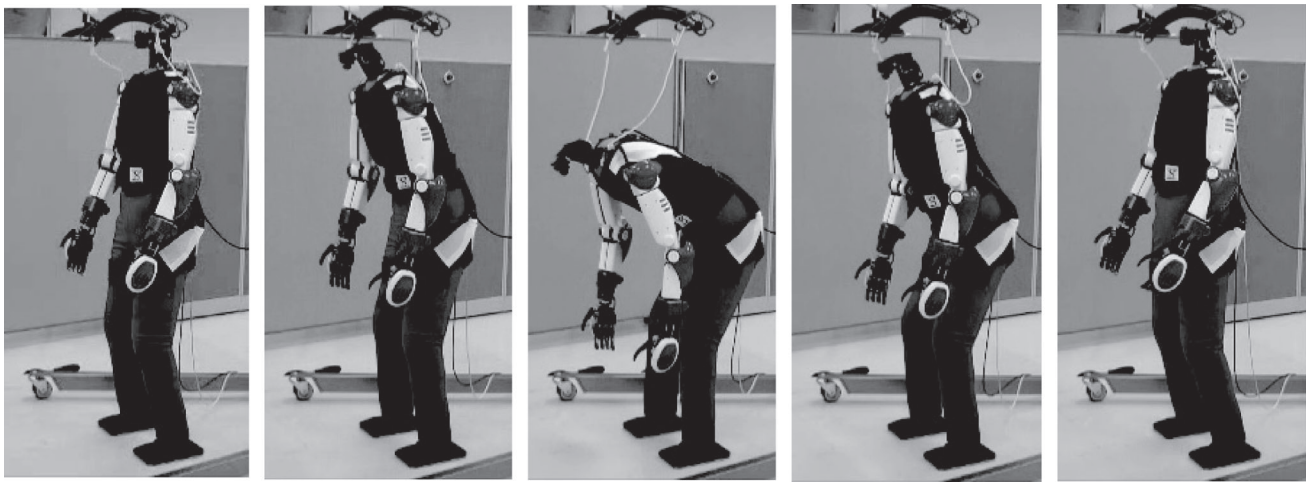

Figure 7. Snapshots of bending motion of HRP-4.

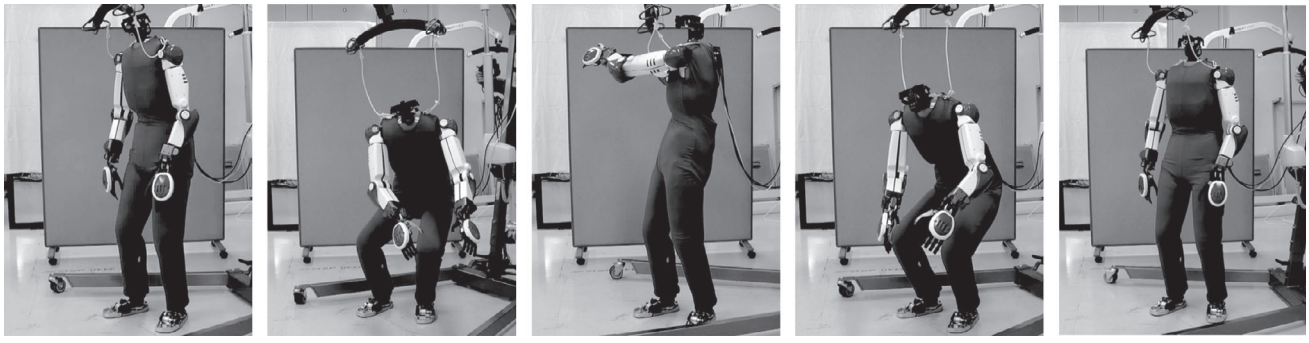

Figure 8. Snapshots of lifting up motion of HRP-4 with twisting its waist.

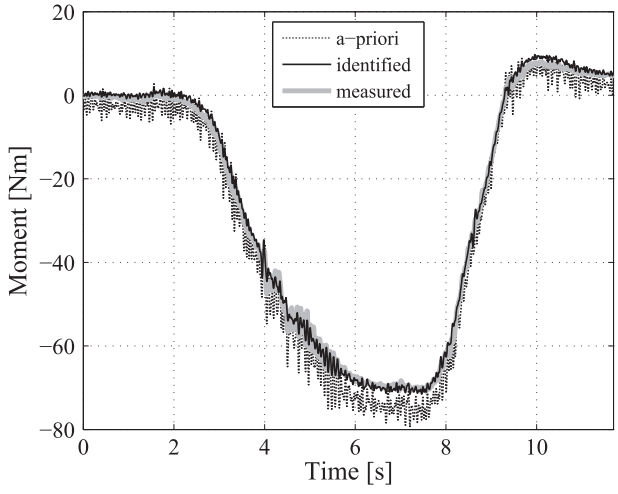

Figure 9. Direct validation of the errors about the moment along pitch-axis of the base link (waist link) when performing bending motion: the measured moment obtained from the force sensors (gray thick line), the moment reconstructed from the dynamics model using the identified parameters (black thin line), and the reconstructed moment with the a priori parameters provided by the manufacturer (black dotted line).

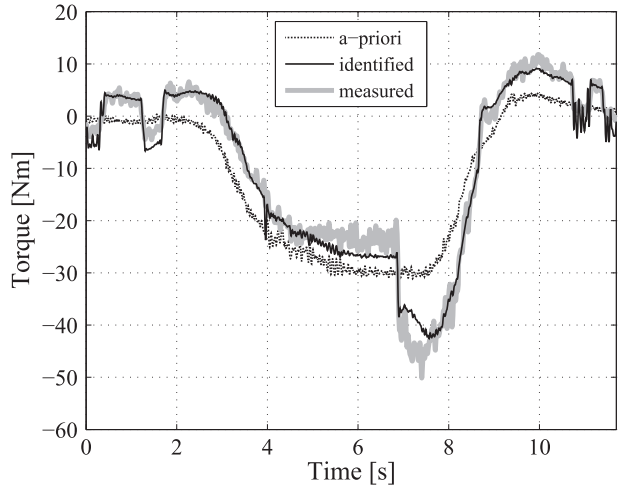

Figure 10. Direct validation of the errors about the torque of the pitch joint of the torso when performing bending motion: the torque obtained from the force sensors and the motor current sensor (gray thick line), the torque reconstructed from the dynamics model using the identified parameters (black thin line), and the reconstructed torque with the a priori parameters provided by the manufacturer (black dotted line).

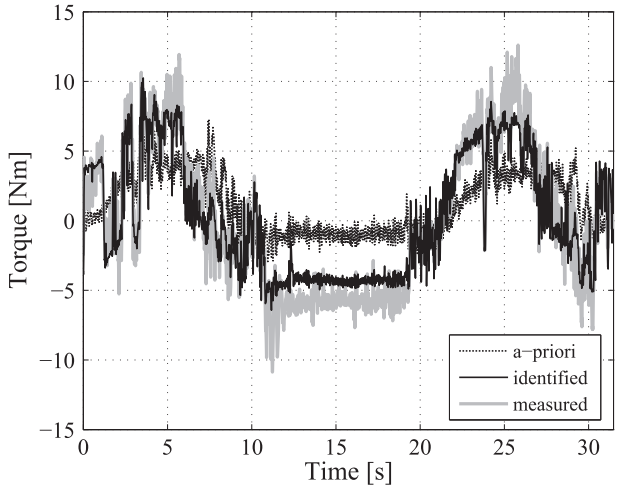

Figure 11. Direct validation of the errors about the torque of the pitch joint of the torso when performing twist motion: line types are the same as in Figure 10.

Figures 10 and 11 show three types of the external and actuator torque acting on the pitch joint of the torso during the bending and twisting motion, respectively. The first one is the torque obtained from the force sensors and the motor current sensor: the lower right-hand side of Equations (5) with (6). In the first case, the parameters of Equation (6) were given by the a priori parameters. The others are those reconstructed from the dynamics model using the identified parameters and the a priori parameters, respectively: the lower left-hand side of Equation (5). The reconstructed torque from the identified model obviously shows a better prediction of the measured one. We also computed RMSE of the reconstruction, which corresponds with $\boldsymbol{e}_j^{(t)}$ in Equation (13). When using the a priori parameters, RMSE are 6.61 Nm (bending motion) and 4.21 Nm (twisting motion). On the other hand, when using the identified parameters, RMSE are smaller: 2.25 Nm (bending) and 1.59 Nm (twisting). All the results show that the identified parameters had better performance rather than the a prior parameters.

5.3. Estimation of the supporting torques of SSL

The converted trajectories were performed by HRP-4 for the following three cases:

- without SSL
- clothing SSL
- clothing SSL with the additional SSL bands (type-(A) in Figure 4 on the back.

In the last case, the additional bands are located so that the stiffness of each wire of type-(A) is equal to double. Let SSL with the additional bands be called 'modified SSL', and SSL without modification be called 'normal SSL'.

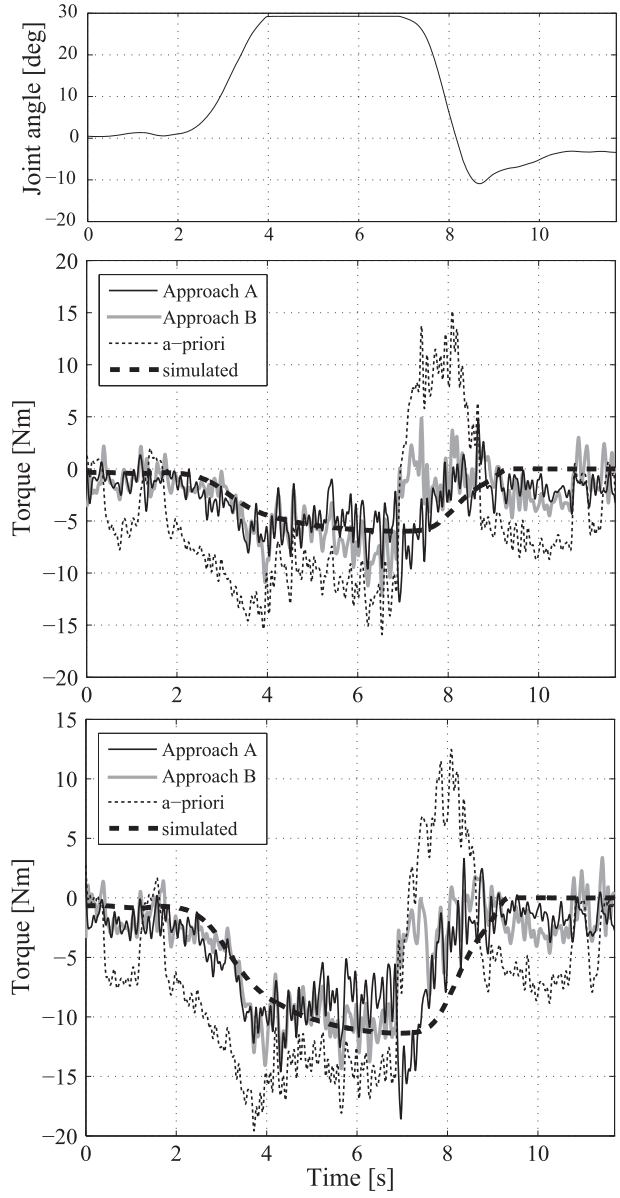

Figure 12. Joint angle trajectory of the torso pitch joint during bending motion (Upper) and comparison of the estimated supporting torques with normal SSL (Middle) and those with modified SSL (Lower). The black thin lines show the supporting torques estimated by approach 3-(A) with the identified values, and the gray thick lines are the torques estimated by approach 3-(B) with the identified values. The black thin dotted lines represent the torque estimated by approach 3-(B) with the a priori values. The black thick dotted line show the torques estimated from the SSL simulation described in section 4. In the case of normal SSL (Middle), RMSE of approach 3-(A) from SSL simulation is 1.97 Nm, RMSE of approach 3-(B) is 2.65 Nm, and RMSE of a priori parameters is 7.42 Nm. In the case of modified SSL (Lower), RMSE of approach 3-(A) from SSL simulation is 2.56 Nm, RMSE of approach 3-(B) is 3.32 Nm, and RMSE of a priori parameters is 7.66 Nm.

The supporting torques of SSL were estimated by the two approaches of step 3 of Section 2, reproduced as follows:

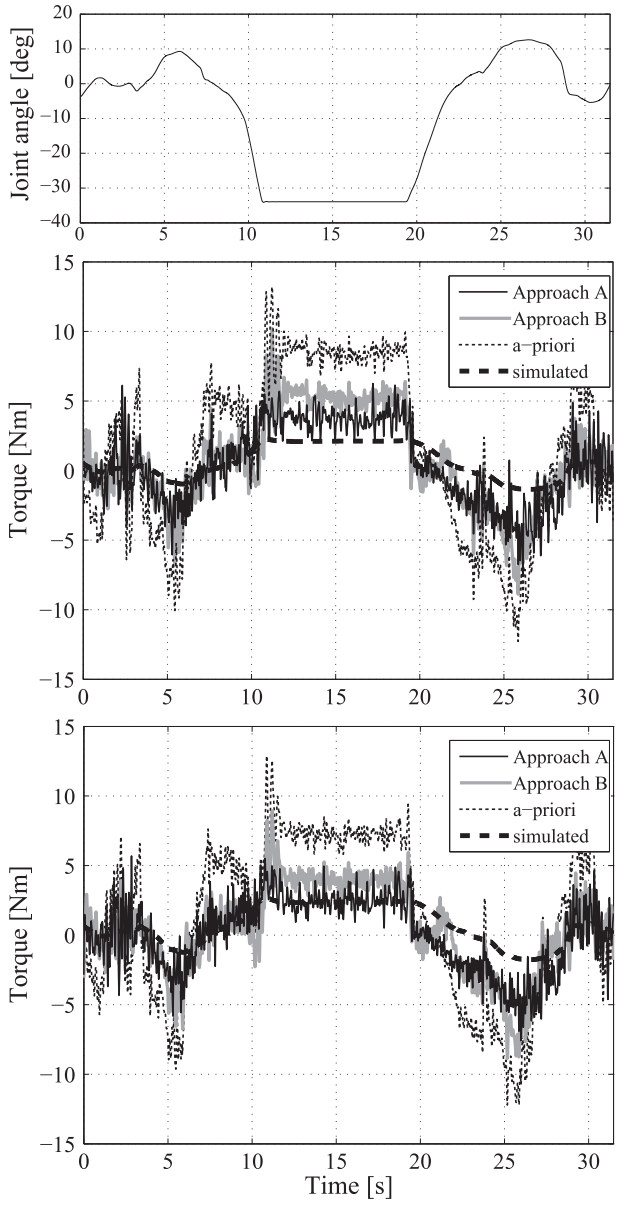

Figure 13. Joint angle trajectory of the torso yaw joint during twisting motion (Upper) and comparison of the estimated supporting (interfering) torques with normal SSL (Middle) and with modified SSL (Lower): line types are the same as in Figure 12. In the case of normal SSL (Middle), RMSE of approach 3-(A) from SSL simulation is 1.84 Nm, RMSE of approach 3-(B) is 2.51 Nm, and RMSE of a priori parameters is 5.08 Nm. In the case of modified SSL (Lower), RMSE of approach 3-(A) from SSL simulation is 1.73 Nm, RMSE of approach 3-(B) is 2.17 Nm, and RMSE of a priori parameters is 4.71 Nm.

- 3-(A). Compute the difference of joint torque between with and without the device: Equation (3)
- 3-(B). Compute the difference between the measured torque and the torque estimated from the model: Equation (4)

We used the identified result $\widehat{\boldsymbol{\phi}}$ and $\widehat{\boldsymbol{\xi}}$ in Section 5.2. The joint torques given by the actuator model including frictions in Equations (3) and (4) were computed as: $\boldsymbol{\tau}_{\text{actuator}}(\boldsymbol{y}, \widehat{\boldsymbol{\xi}}) = \boldsymbol{Z}\widehat{\boldsymbol{\xi}}$. The joint torques coming from the dynamics of the kinematic chain were: $\boldsymbol{\tau}_{\text{dyn}}(\boldsymbol{x}, \widehat{\boldsymbol{\phi}}) = \boldsymbol{Y}_j\widehat{\boldsymbol{\phi}} - \boldsymbol{F}_j$. When there exist external forces, we assumed that $\boldsymbol{\tau}_{\text{dyn}}$ includes external joint torques $\boldsymbol{F}_j$.

Figure 12 shows the comparison of the supporting torques of the pitch joint of the torso during bending motion, and Figure 13 shows that of the yaw joint of the torso during twisting motion. In both Figures 12 and 13, the upper figures show the joint trajectory, the middle figures show the supporting torques with normal SSL, and the lower figures show those with modified SSL. The line types are mentioned in the caption of Figure 12.

In Figure 12, we could recognize the effect which reduce the original joint torques in 10. In the case of bending motion, the supporting torques of the SSL wires of type-(A) in Figure 4 are dominant, and the wires of type-(B) had little influence. It leads that the supporting torques doubled when clothing the modified SSL with the doubled stiffness of type-(A) wires. Since the ground-truth value of the stiffness of type-(A) wire is known, the simulated torques can be regarded as reliable values. The values could be predicted by approach 3-(A) and 3-(B) with identification, and not estimated by the a priori values, as shown in Figure 12.

Figure 13 showed that SSL interfered the movement along the yaw direction. In this sense, SSL does not support for the movement of the yaw joint of the torso. The black thin lines show the correlation with the gray thick line; however, the amplitude of the black thin line is larger than that of the black thick dotted line. We can see that the interfering torques did not change when clothing the modified SSL with the doubled stiffness of type-(A) wires. In the case of twisting motion, interfering torques of the SSL wires of type-(B) are dominant, and the wires of type-(A) had little influence. As the ground-truth value of the stiffness of type-(B) wire is actually unknown and SSL has several components like a belt and some buckle to guide the wires around the waist, the simulated torques are not necessarily true. Though the results are expected to be feedback to the modeling of SSL in future work, we don't detail in modeling and designing of SSL because they are out of scope of the paper.

5.4. Identification of SSL

Finally, we check the accuracy of the torques estimated from the proposed scheme. We identified the stiffness of SSL bands from the estimated torques, and compare the dentified value with the ground-truth stiffness. We know the ground-truth stiffness of type-(A) wire, and its supporting torques are dominant during bending motion.

Table 2. Comparison of the stiffness of the normal SSL band.

	Stiffness (N/m) (error from (a))
(a) Ground-truth stiffness	197.8
(b) Identified by approach 3-(A)	185.8(6.1%)
(c) Identified by approach 3-(B)	181.3(8.3%)
(d) Identified with a priori model	65.8(66.7%)

Table 3. Comparison of the stiffness of the modified SSL band.

	Stiffness (N/m) (error from (a))
(a) Ground-truth stiffness	395.6
(b) Identified by approach 3-(A)	364.6(7.9%)
(c) Identified by approach 3-(B)	331.5(16.2%)
(d) Identified with a priori model	207.1(47.8%)

So, we identified the stiffness of only type-(A) wires from the estimated supporting torques of Figure 12.

The stiffness and the natural length of each SSL band were identified by solving Equation (26). We added the constraint such that the stiffness of each wire is same because of the symmetry; on the other hand, the natural lengths are different among the wires. Table 2 shows the result of the identified stiffness of the normal SSL band: (a) the ground-truth stiffness, (b) the identified value using the supporting torque estimated from approach 3-(A), (c) the identified one by approach 3-(B), and (d) the identified one using the torque estimated from the a priori values. Table 3 also shows the result of the identified stiffness of the modified SSL band whose stiffness doubled.

Tables 2 and 3 show that the proposed scheme could successfully identify the mechanical property of the device.

The two errors of approach (A) are within 10%, which means that the propose scheme estimate the supporting effect accurately. Though there is the strict constraint such that the same motion has to be performed between with and without the device, the approach (A) showed better performance than (B). Though the error of approach (B) in Table 2 is almost same as that of (A), the error of approach (B) in Table 3 is not small with respect to the others. That is mainly because there is the error peak, especially when the joint starts to move around at $t = 7\,\mathrm{s}$ as shown in Figures 10 and 12, because the current friction model cannot eliminate Stribeck effect [26], which is usually seen at low speeds. However, while a joints is completely stopping or moving at above certain speeds, the nonlinear effect does not appear on the friction. Since we identified both the static and dynamic friction, approach (B) can estimate the supporting torques, while the joint stops or moves at above certain speeds, as shown in Figures 10 and 12. To exploit the advantage of approach (B) which needs only the motions with devices, practical identification considering Stribeck effect as shown in the applications for industrial manipulators [27,28] will be addressed in our future work.

6. Conclusion

This paper presented the new application of a humanoid robot as an evaluator of assistive devices. The basic flow of the proposed frame work is as follows. The motions of a human are, at first, measured by motion capturing. They are converted to those of a humanoid robot by using the retargeting technique. The robot performs the retargeted motions with supported by an assistive device. The supporting effect of the device is estimated from its sensor data.

We also showed the two approaches to estimate supporting torques from the sensor data. Approach (A) measures the joint torques when the robot performs the exact same joint trajectories with and without a device, respectively, and extract the difference between the two. Approach (B) measures the joint torques only when the robot is wearing a device, and computes the difference from the torques estimated from the inverse dynamics model of the robot. Though approach (A) requires the two measurements under the constraint that the exact same motion has to be repeated between the two, it can cancel the unmodeled friction forces and tends to be more accurate than approach (B). On the other hand, after inertial parameters identification without a device, approach (B) can estimate the supporting effect only from the measurement with a device. The motion used in the identification does not need to be exact same as the motion used for estimating the supporting effect.

In order to enhance the evaluation of the proposed framework, we also utilize the identification of mechanical properties of a humanoid robot. In this paper, we combined the method of identification based on the base-link dynamics and joint-dynamics to estimate inertial

parameters, several friction parameters, and motor constants simultaneously.

We introduce the general modeling scheme of passive assistive devices for simulation by using the formulation of wire driven multi-body systems. We also showed the methodology of the identification of the model parameters of the simulation from the experimental data, which enable to make simulations reflect the real situations, for example, to test product configurations.

According to the proposed scheme, we evaluated the supporting torques of a passive assistive wear 'Smart Suit Lite (SSL)' as an example of assistive device, and utilized HRP-4 as the humanoid platform. We recorded two types of the motion: with bending forward and twisting waist, respectively. The motions were retargeted to playback by HRP-4, and the mechanical properties of the robot were also identified.

After identifying, the supporting torques were estimated by the three ways: the proposed two approaches and the estimation using the simulation model with a priori parameters provided by manufacturers. In both approaches, the estimated supporting torques show the good correlation with the simulation result of SSL along the pitch axis with the ground-truth stiffness; on the other hand, when using a priori parameters, the estimated supporting torques did not match the simulated torques at all. Though the patterns of the trajectory about the interfering torques during the twisting motion are similar between the estimated ones and the simulation model, the amplitudes of them are different. Since the simulation model about SSL along the yaw axis is not well investigated, this difference of the results is expected to be feedback to the modeling of SSL.

In order to check the accuracy of the torques estimated from the proposed scheme, the estimated supporting torques were also used to identify the stiffness of SSL band and compare it to the ground-truths value. The proposed scheme could successfully identify the mechanical property of the device. Approach (A) showed better performance than approach (B), because approach (B) requires the many mechanical parameters and contains unmodeled friction forces. However, there is the strict constraint in approach (A) such that the same motion has to be performed between with and without the device. If the supporting effect is relatively large with respect to the servo torques of a robot, it is difficult to keep exact same trajectories between with and without the device. The error of approach (B) is not small currently, which seems to come mainly from the nonlinear friction at low speeds; on the other hand, the approach (B) could estimate the supporting torques accurately, while the joint stops or moves at above certain speeds. Therefore, when evaluating fast motions, approach (B) will be useful because of the difficulty of repeating the same trajectories in approach (A).

Disclosure statement

No potential conflict of interest was reported by the authors.

Funding

This research was supported by Project to Promote the Development and Introduction of Robotic Devices for Nursing Care funded by METI/AMED; JSPS KAKENHI [grant number 25820082].

Notes on contributors

Ko Ayusawa received the BS degree in mechanical engineering, and the MS and PhD degrees in mechano-informatics from the University of Tokyo, Japan, in 2006, 2008, and 2011, respectively. He worked with the Department of Mechano-Informatics at the University of Tokyo, as a postdoctoral researcher from 2011 to 2012, and as a project assistant processor in 2013. He is currently a researcher of Intelligent Systems Research Institute, National Institute of Advanced Industrial Science and Technology (AIST), Tsukuba, Japan, and a researcher of CNRS-AIST JRL (Joint Robotics Laboratory), UMI3218/RL. His research interests include identification of human/humanoid dynamics, motion control for humanoid robots, and kinematics and dynamics simulation for human musculoskeletal models.

Eiichi Yoshida received ME and PhD degrees on Precision Machinery Engineering from Graduate School of Engineering, the University of Tokyo in 1993 and 1996, respectively. In 1996, he joined former Mechanical Engineering Laboratory, later reorganized as National Institute of Advanced Industrial Science and Technology (AIST), Tsukuba, Japan. He served as Co-Director of AIST/IS-CNRS/ST2I Joint French-Japanese Robotics Laboratory (JRL) at LAAS-CNRS, Toulouse, France, from 2004 to 2008. Since 2009, he is Co-Director of CNRS-AIST JRL (Joint Robotics Laboratory), UMI3218/RL, and since 2015 he serves as Deputy-Director of Intelligent Systems Research Institute (IS-AIST), AIST, Tsukuba, Japan. His research interests include robot task and motion planning, human modeling, and humanoid robots.

Yumeko Imamura received Master of Information Science and Technology and PhD in the field of Systems Science and Informatics from Graduate School of Information Science and Technology, Hokkaido University in 2011 and 2014, respectively. She served as a research fellow of Japan Society for the Promotion of Science at Hokkaido University, Sapporo, Japan, from 2014 to 2015. Since 2015, she is researcher of CNRS-AIST Joint Robotics Laboratory, UMI3218/RL, and Intelligent Systems Research Institute (IS-AIST), National Institute of

Advanced Industrial Science and Technology (AIST), Tsukuba, Japan. Her research interests include biomechanics, human modeling, and power assistive technologies.

Takayuki Tanaka received the BC degree in 1994, the MS degree in 1996, and the PhD degree, respectively, from the University of Electro-Communications (UEC). He was an assistant professor of Department Mechanical and Control Engineering of UEC from April 1996 to March 2003. During this period, he was also a visiting researcher of University of California, Irvine through October 2001 to March 2002. He became an associate professor of UEC in April 2003. Since April 2004, he is currently an associate professor of Graduate School of Information Science and Technology of Hokkaido University. His major research topics are assistive robot, wearable robot and human sensing. He is a member of RSJ, SICE, IEEE, and a fellow member of JSME.

References

[1] Sankai Y. HAL: hybrid assistive limb based on cybernics. In: Kaneko M, Nakamura Y, editors. Robotics research, Springer tracts in advanced robotics. Vol. 66. Berlin: Springer; 2011. p. 25–34.

[2] Imamura Y, Tanaka T, Suzuki Y, et al. Motion-based-design of elastic material for passive assistive device using musculoskeletal model. J. Rob. Mech. 2011;23:58–66.

[3] Nakamura Y, Yamane K, Fujita Y, et al. Somatosensory computation for man–machine interface from motion-capture data and musculoskeletal human model. IEEE Trans. Rob. 2005;21:58–66.

[4] Miura K, Yoshida E, Kobayashi Y, et al. Humanoid robot as an evaluator of assistive devices. In: Proceedings of the IEEE International Conference on Robotics and Automation; Karlsruhe, Germany; 2013. p. 671–677.

[5] Kaneko K, Kanehiro F, Morisawa M, et al. Cybernetic human HRP-4C. In: Proceedings of the IEEE-RAS International Conference on Humanoid Robots; Paris, France; 2009. p. 7–14.

[6] Kaneko K, Kanehiro F, Morisawa M, et al. Humanoid robot HRP-4 – humanoid robotics platform with lightweight and slim body. In: Proceedings of the IEEE/RSJ International Conference on Intelligent Robots and Systems; San Francisco, CA; 2011. p. 4400–4407.

[7] Santaguida PL, Pierrynowski M, Goldsmith C, et al. Comparison of cumulative low back loads of caregivers when transferring patients using overhead and floor mechanical lifting devices. Clin. Biomech. 2005;20:906–916.

[8] Gleicher M. Retargetting motion to new characters. In: Proceedings of the 25th Annual Conference on Computer Graphics and Interactive Techniques. SIGGRAPH'98; Orlando, FL; 1998. p. 33–42.

[9] Nakaoka S, Nakazawa A, Kanehiro F, et al. Learning from observation paradigm: leg task models for enabling a biped humanoid robot to imitate human dances. Int. J. Rob. Res. 2007;26:829–844.

[10] Miura K, Morisawa M, Nakaoka S, et al. Robot motion remix based on motion capture data towards human-like locomotion of humanoid robots. In: Proceedings of the IEEE-RAS International Conference on Humanoid Robots; Paris, France; 2009. p. 596–603.

[11] Khalil W, Dombre E. Modeling, identification and control of robots. London: Hermès Penton; 2002.

[12] Ayusawa K, Nakaoka S, Yoshida E, et al. Evaluation of assistive devices using humanoid robot with mechanical parameters identification. In: Proceedings of the IEEE-RAS International Conference on Humanoid Robots; Madrid, Spain; 2014. p. 205–211.

[13] Kusaka T, Tanaka T, Kaneko S, et al. Assist force control of smart suit for horse trainer considering motion synchronization and postural stabilization. In: Proceedings of ICCAS-SICE; Fukuoka, Japan; 2009. p. 770–775.

[14] Imamura Y, Tanaka T, Shibukawa F. Investigations of needs for KEIROKA assistive technology in field of nursing care in Denmark and Japan. Proceedings of the 2nd International Conference on Universal Village; Boston, MA; 2014. D2S1PM-1-4.

[15] Venture G, Ayusawa K, Nakamura Y. Optimal estimation of human body segments dynamics using realtime visual feedback. In: Proceedings IEEE/International Conference on Intelligent Robot System; St. Louis, MO; 2009. p. 1627–1632.

[16] Albu-Schäffer A, Haddadin S, Ott C, et al. The DLR lightweight robot: design and control concepts for robots in human environments. Ind. Rob. 2007;34:376–385.

[17] Atkeson CG, An CH, Hollerbach JM. Estimation of inertial parameters of manipulator loads and links. Int. J. Rob. Res. 1986;5:101–119.

[18] Ayusawa K, Venture G, Nakamura Y. Identifiability and identification of inertial parameters using the underactuated base-link dynamics for legged multibody systems. Int. J. Rob. Res. 2014;33:446–468.

[19] Yoshida K, Nenchev D, Uchiyama M. Moving base robotics and reaction management control. In: Proceedings of the 7th International Symposium of Robotics Research; Munich, Germany; 1995. p. 100–109.

[20] Mayeda H, Yoshida K, Osuka K. Base parameters of manipulator dynamic models. IEEE Trans. Rob. Autom. 1990;6:312–321.

[21] Gautier M, Khalil W. Exciting trajectories for the identification of base inertial parameters of robots. Int. J. Rob. Res. 1992;11:363–375.

[22] Yoshida K, Khalil W. Verification of the positive definiteness of the inertial matrix of manipulators using base inertial parameters. Int. J. Rob. Res. 2000;19:498–510.

[23] Gautier M, Venture G. Identification of standard dynamic parameters of robots with positive definite inertia matrix. In: Proceedings of the IEEE/RSJ International Conference on Intelligent Robots and Systems; Tokyo, Japan; 2013. p. 5815–5820.

[24] Ayusawa K, Ikegami Y, Nakamura Y. Simultaneous global inverse kinematics and geometric parameter identification of human skeletal model from motion capture data. Mech. Mach. Theory. 2014;74:274–284.

[25] Ayusawa K, Morisawa M, Yoshida E. Motion retargeting for humanoid robots based on identification to preserve and reproduce human motion features. In: Proceedings of the IEEE/RSJ International Conference on Intelligent Robots and Systems; Hamburg, Germany; 2015. p. 2774–2779.
[26] Armstrong-Hélouvry B, Dupont P, Wit CCD. A survey of models, analysis tools and compensation methods for the control of machines with friction. Automatica. 1994;30:1083–1138.
[27] Jamisola R, Ang MH, Khatib O, Oetomo DN, Lim TM, Lim SY. Compliant motion using a mobile manipulator: an operational space formulation approach to aircraft canopy polishing. Int. J. Adv. Rob. 2005;19:613–634.
[28] Hamon P, Gautier M, Garrec P. New dry friction model with load- and velocity-dependence and dynamic identification of multi-DOF robots. In: Proceedings of the IEEE International Conference on Robotics and Automation; Shanghai, China; 2011. p. 1077–1084.